J|A|C|S ARTICLES

Published on Web 06/11/2009

Intrinsic Dipole-Field-Driven Mesoscale Crystallization of Core−Shell ZnO Mesocrystal Microspheres

Z. Liu,[†] X. D. Wen,[†] X. L. Wu,*[,†] Y. J. Gao,[†] H. T. Chen,[†] J. Zhu,[†,§] and P. K. Chu*[,‡]

Nanjing National Laboratory of Microstructures, Nanjing University, Nanjing 210093, People's Republic of China, Department of Physics and Materials Science, City University of Hong Kong, Tat Chee Avenue, Kowloon, Hong Kong, and College of Physics Science and Technology, Yangzhou University, Yangzhou 225002, People's Republic of China

Received May 14, 2009; E-mail: hkxlwu@nju.edu.cn (X.L.W.); paul.chu@cityu.edu.hk (P.K.C.)

Abstract: Novel uniform-sized, core−shell ZnO mesocrystal microspheres have been synthesized on a large scale using a facile one-pot hydrothermal method in the presence of the water-soluble polymer poly(sodium 4-styrenesulfonate). The mesocrystal forms via a nonclassical crystallization process. The intrinsic dipole field introduced by the nanoplatelets as a result of selective adsorption of the polyelectrolyte on some polar surfaces of the nanoparticles acts as the driving force. In addition, it plays an important role throughout the mesoscale assembly process from the creation of the bimesocrystalline core to the apple-like structure and finally the microsphere. Our calculation based on a dipole model confirms the dipole-field-driven mechanism forming the apple-like structure.

1. Introduction

The use of colloidal nanocrystals as the building units to produce self-assembled and highly ordered superstructures has become attractive in materials design and biomineralization recently.[1−16] To precisely control the structure and morphology of the products, a thorough understanding of the crystallization process is imperative. There are generally two pathways with regard to the crystallization process.[11−15] The first one is so-called classical crystallization in which the crystal grows on the stable nuclei via ion-by-ion addition and unit replication. The second one is nonclassical crystallization in which the crystal forms via a particle-mediated process, namely aggregation, self-assembly, and mesoscopic transformation of the nanoparticles coupled with a restructuring process on a length scale between 1 nm to 1 μm. From the perspective of the "bottom-up" approach, the nonclassical crystallization pathway constitutes a facile strategy to fabricate ordered superstructures and has become a topic of intensive research.

There are two main mechanisms in nonclassical crystallization: oriented attachment and mesocrystallization. Oriented attachment is described as the spontaneous assembly of adjacent particles with common crystallographic orientations by crystallographic fusion at the planar interface.[10] Reduction of the surface free energy by fusing and eliminating the high-energy surfaces drives spontaneous assembly. A new class of alternative crystals, mesocrystals, has recently been introduced by Cölfen et al.[15] The mesocrystal is a colloidal crystal composed of individual nonspherical nanocrystals sharing the same crystallographic structure with interspersed organic additives. It exhibits a scattering pattern resembling that of a single crystal. Since the mesocrystal introduces a new possibility to control the crystal morphology by using the anisotropic building units, it has large potential in biomineralization and construction of complex materials.[11−16] Currently, there are three possible ways in the 3D alignment forces for the formation of the mesocrystal,[14] but the detailed mechanisms are still largely not understood.

The wurtzite ZnO crystal, a multifunctional material, is constructed by a number of alternating planes stacked along the *c*-axis direction. As the planes consist of tetrahedrally coordinated Zn^{2+} and O^{2-} ions, the structure produces the Zn^{2+} terminated (0001) face and O^{2-} terminated $(000\bar{1})$ face and possesses an intrinsic dipole moment along the *c*-axis. Based on the vapor−liquid−solid growth model, Wang et al. suggest that this dipole characteristic will drive a self-coiling process

[†] Nanjing University.
[‡] City University of Hong Kong.
[§] Yangzhou University.

(1) Whitesides, G. M.; Grzybowski, B. *Science* **2002**, *295*, 2418–2421.
(2) Li, M.; Schnablegger, H.; Mann, S. *Nature* **2000**, *404*, 59–61.
(3) Mann, S. *Biomineralization, Principles and Concepts in Bioinorganic Materials Chemistry*; Oxford University Press: Oxford, 2001.
(4) Kniep, R.; Busch, S. *Angew. Chem., Int. Ed.* **1996**, *35*, 2624–2628.
(5) Xia, Y. N.; Gates, B.; Yin, Y. D.; Lu, Y. *Adv. Mater.* **2000**, *12*, 693–713.
(6) Yin, Y. D.; Alivisatos, A. P. *Nature* **2005**, *437*, 664–670.
(7) Tian, Z. R. R.; Voigt, J. A.; Liu, J.; McKenzie, B.; McDermott, M. J.; Rodriguez, M. A.; Konishi, H.; Xu, H. F. *Nat. Mater.* **2003**, *2*, 821–826.
(8) Yang, G. H.; Zeng, H. C. *Angew. Chem., Int. Ed.* **2004**, *43*, 5930–5933.
(9) Alivisatos, A. P. *Science* **2000**, *289*, 736–737.
(10) Penn, R. L.; Banfield, J. F. *Science* **1998**, *281*, 969–971.
(11) Cölfen, H.; Mann, S. *Angew. Chem., Int. Ed.* **2003**, *42*, 2350–2365.
(12) Niederberger, M.; Cölfen, H. *Phys. Chem. Chem. Phys.* **2006**, *8*, 3271–3287.
(13) Meldrum, F. C.; Cölfen, H. *Chem. Rev.* **2008**, *108*, 4332–4432.
(14) Cölfen, H.; Antonietti, M. *Mesocrystals and Nonclassical Crystallization*; John Wiley & Sons: Chichester, U.K., 2008.
(15) Cölfen, H.; Antonietti, M. *Angew. Chem., Int. Ed.* **2005**, *44*, 5576–5591.
(16) Zhou, L.; O'Brien, P. *Small* **2008**, *4*, 1566–1574.

to form a nanobelt or ring structure.[17,18] However, in the solution synthesis, the situation is different. Theoretical calculation indicates that an anisotropic charged object can generate a screened electrostatic potential that is anisotropic at any distance.[19] Such a potential can be applied as the driving force to achieve mutual alignment of the building units to form an anisotropic superstructure.[20,21] Recently, by using electron holography, Kniep et al. have furnished direct experimental proof demonstrating the important role of the electric field in the formation of the fluoroapatite mesocrystals in gelatin.[22] Mo et al. and Li et al. have synthesized in ZnO the mesocrystal tubular ZnO hollow structures in which the dipole-induced electrostatic interactions between the building units act as the aligning force.[23,24] However, detailed reports on the ZnO mesocrystal have heretofore been quite scarce, and the dipole-field-induced ZnO mesocrystals are all assembled along the *c*-axis forming anisotropic superstructures. In this paper, we report a low-temperature, polymer-mediated, and one-pot hydrothermal synthesis of a unique core−shell-structured ZnO mesocrystal microsphere superstructure constructed by densely packed nanoplatelets. The polyelectrolyte poly(sodium 4-styrenesulfonate) used to modify the crystal growth process is believed to retain a permanent dipole field moment by selective adsorption on some polar faces. The new nanoplatelet-based, core−shell mesocrystal microsphere formed under the synergistic effects of the electric fields of the core and the dipole−dipole interaction between the nanoplatelets on the shell is a good example of a dipole-field-induced superstructure, which is expected to have applications in photocatalysis and play an important role in the photoluminescence properties of doped ZnO.[25,26] The process described here also provides an alternative pathway to fabricate core−shell superstructures other than Ostwald ripening[27] or the well-known "Layer By Layer" assembly method.[28,29]

2. Experimental Section

Preparation of ZnO Mesocrystals. The chemicals, hexamethylene tetramine (HMT), $Zn(NO_3)_2 \cdot 6H_2O$, and poly(sodium 4-styrenesulfonate) (PSS, average molecular weight $M_w \approx 100\,000$ g mol^{-1}, solid content: 20%), were analytical grade and used as received without further purification. In the typical synthesis, 0.002 mol of $Zn(NO_3)_2 \cdot 6H_2O$ and 5 mL of PSS were dissolved together in 30 mL of deionized water with stirring for 5 min. Then, 0.002 mol of HMT was added to the above solution. The mixture immediately became milky and was stirred for another 10 min. The solution was transferred to a 35 mL Teflon-lined stainless autoclave and maintained at 95 °C for 30 min to 10 h, respectively. Afterward, the autoclave was air-cooled to room temperature. The 30-min sample was a cloudy solution (white floccules), and the 1 h sample contained a mixture of cloudy solution and white precipitates, but the other samples were pure white precipitates. These samples were treated by centrifugation and then thoroughly rinsed with deionized water and ethanol several times, before drying at 60 °C in an oven for subsequent characterization.

Characterization. The phases and structure of the synthesized products were examined by XRD on a Rigaku 3015 with Cu Kα radiation ($\lambda = 1.5418$ Å). The patterns were analyzed by the Scherrer formula to estimate the coherence length D_{hkl}. The parameter k here is equal to 0.9 (a constant between 0.8 to 1.4). Full widths at half-maxima (fwhm) and background correction were done by using OriginLab Origin 7.5. The morphologies and sizes of the products were characterized by field-emission scanning electron microscopy (FESEM) (JEOL JSM-7000F or FEG JSM 6335). The detailed microstructures of the products were evaluated by transmission electron microscopy (Tecnai G2 20 S-TWIN and JEOL JEM-4000EX at 200 kV). Thermogravimetric analysis (TGA) was carried out on a Pyris 1 TGA (PerkinElmer Corp.) under a nitrogen atmosphere at a scanning rate of 10 °C min^{-1} from room temperature to 700 °C. Optical microscopy (Nikon Eclipse 80i) was utilized to observe the stained samples.

3. Results and Discussion

The powder X-ray diffraction (p-XRD) pattern of a representative powder product precipitated for 10 h is shown in Figure SI-1 in the Supporting Information. The as-synthesized powder has a pure hexagonal wurtzite phase according to the JCPDS card no. 36-1451 with a space group of $P6_3mc$ and lattice parameters of $a = 3.25$ Å and $c = 5.21$ Å. We have found that the relative intensity ratios of the (100)/(002) and (101)/(002) reflections are larger than the standard values in the JCPDS card no. 36-1451, especially for the (100)/(002) ratio, indicating preferential orientation growth in the (100) direction. Furthermore, detailed analysis of the peak broadening using the Scherrer equation shows the coherence lengths of D_{hkl} of the (100) and (002) reflections to be $D_{100} = 37.5$ nm and $D_{002} = 15.1$ nm. D_{100} is larger than D_{002} and the D_{100}/D_{002} ratio is 2.45, which is similar to that reported by Taubert et al. in the polymer-mediated ZnO growth.[30] The significant reduction in D_{002} suggests that the polymer controls the crystallite morphology by preferential adsorption on the basal plane.[30−32] According to the calculated ratio, it is expected that the primary crystallites will take up a sheet- or plate-like shape in the final ZnO superstructure. Furthermore, a polymer content loss of ∼3% during the TGA of this sample supports adsorption of the polymer onto the nanocrystals.

Figure 1 shows the field emission scanning electron microscopy (FESEM) images of the ZnO mesocrystal microspheres. The low-magnification images reveal that the products consist of microspheres with a nearly uniform size distribution (Figure 1a and 1b). The average diameter of the ZnO microspheres is ∼5.5 μm, and their shapes are not fully spherical. To further determine the detailed structure of the microspheres, the high-magnification FESEM images are presented in Figure 1c and 1d. The whole microsphere surface is composed of densely packed nanoplatelets aligned perpendicularly to the sphere

(17) Kong, X. Y.; Wang, Z. L. *Nano Lett.* **2003**, *3*, 1625–1631.
(18) Kong, X. Y.; Ding, Y.; Yang, R.; Wang, Z. L. *Science* **2004**, *303*, 1348–1351.
(19) Agra, R.; Wijland, F. V.; Trizac, E. *Phys. Rev. Lett.* **2004**, *93*, 018304.
(20) Wang, T. X.; Antonietti, M.; Cölfen, H. *Chem.—Eur. J.* **2006**, *12*, 5722–5730.
(21) Wohlrab, S.; Pinna, N.; Antonietti, M.; Cölfen, H. *Chem.—Eur. J.* **2005**, *11*, 2903–2913.
(22) Simon, P.; Zahn, D.; Lichte, H.; Kniep, R. *Angew. Chem., Int. Ed.* **2006**, *45*, 1911–1915.
(23) Mo, M. S.; Lim, S. H.; Mai, Y. W.; Zheng, R. K.; Ringer, S. P. *Adv. Mater.* **2008**, *20*, 339–342.
(24) Li, Z. H.; Geβner, A.; Richters, J. P.; Kalden, J.; Voss, T.; Kübel, C.; Taubert, A. *Adv. Mater.* **2008**, *20*, 1279–1285.
(25) Jang, E. S.; Won, J.-H.; Hwang, S.-J.; Choy, J.-H. *Adv. Mater.* **2006**, *18*, 3309–3312.
(26) Zeng, X. Y.; Yuan, J. L.; Wang, Z. Y.; Zhang, L. D. *Adv. Mater.* **2007**, *19*, 4510–4514.
(27) Liu, B.; Zeng, H. C. *Small* **2005**, *5*, 566–571.
(28) Caruso, F.; Lichtenfeld, H.; Giersig, M.; Möhwald, H. *J. Am. Chem. Soc.* **1998**, *120*, 8523–8524.
(29) Caruso, F.; Caruso, R. A.; Möhwald, H. *Science* **1998**, *282*, 1111–1114.
(30) Taubert, A.; Kübel, C.; Martin, D. C. *J. Phys. Chem. B* **2003**, *107*, 2660–2666.
(31) Taubert, A.; Plams, D.; Weiss, O.; Piccini, M.-T.; Batchelder, D. N. *Chem. Mater.* **2002**, *14*, 2594–2601.
(32) Taubert, A.; Glasser, G.; Palms, D. *Langmuir* **2002**, *18*, 4488–4494.

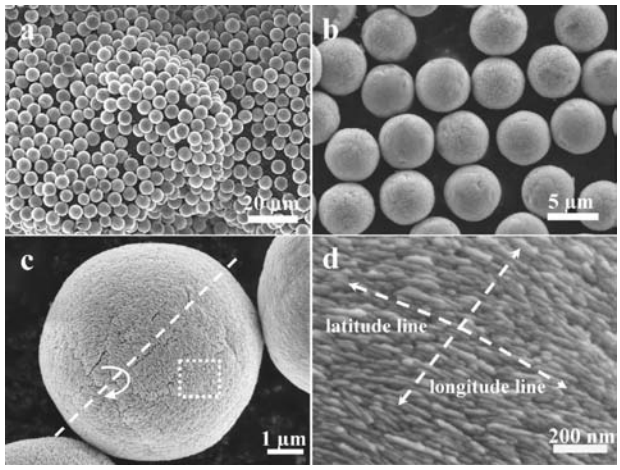

Figure 1. FESEM images of the ZnO mesocrystal microspheres with a synthesis time of 10 h. (a and b) Two low-magnification sphere morphologies of the sample. (c) An enlarged single microsphere. (d) High magnification image of a microsphere (marked with a dashed rectangle in (c)). It reveals the detailed structure of the surface.

pointing to the same center. These nanoplatelets are not connected to each other. They are arranged regularly instead of disorderly on the surface. The 10−20 nm thick nanoplatelets, which are in agreement with the coherence length calculation based on the p-XRD analysis, make up the microspheres. Here, if we imagine that the microsphere is the "earth", the dashed line in Figure 1c is the axis of the "earth". The nanoplatelets are stacked along the longitudinal line from the equator to the pole on the "earth's" surface. They are parallel to each other along the longitudinal line and are aligned from end to end along the latitude line. The rough surface and orderly arranged nanoplatelets strongly suggest that the crystallization mechanism of the microsphere is not ion-by-ion but instead a nonclassical crystallization process.[11−16]

The transmission electron microscopy (TEM) and [0001] zone-axis high resolution TEM (HRTEM) images taken on the ultrathin section of the microsphere rim (marked in Figure 2a) provide further information on the crystallization. It can be observed from Figure 2a that the solid microsphere has an almost hexagonal shape with rounded corners. The [0001] zone-axis selected area electron diffraction (SAED) pattern in Figure 2b discloses that the nanoplatelets grow normal to the [0001] direction. The single crystal-like pattern consisting of individual diffraction spots indicates that the whole assembly of the building units is highly oriented and aligned. The results also suggest that there is a narrow range of small angle lattice mismatch between the boundaries of the nanoparticles when assembling in the same orientation. This is a typical situation in mesocrystal assembly.[11−16] The HRTEM image in Figure 2c shows the detailed arrangement of the nanoplatelets. The lattice fringes are observed to have a spacing of 0.28 nm corresponding to the interplanar spacing of $(01\bar{1}0)$ plane of ZnO (Figure 2b). This implies that well crystallized small nanocrystallites make up the thin nanoplatelets. The parallel lattice fringes indicate that the nanoplatelets are well aligned in a common crystallographic fashion, which is in good agreement with the SEM results (Figure 1d). At the same longitude, they share the same crystallographic direction with the (0001) top/bottom polar faces parallel to each other. At the same latitude, they are also well aligned. The existence of mesopores (or amorphous, defect regions) during the assembly characteristic of the mesocrystal is clearly observed in the HRTEM image (dashed white

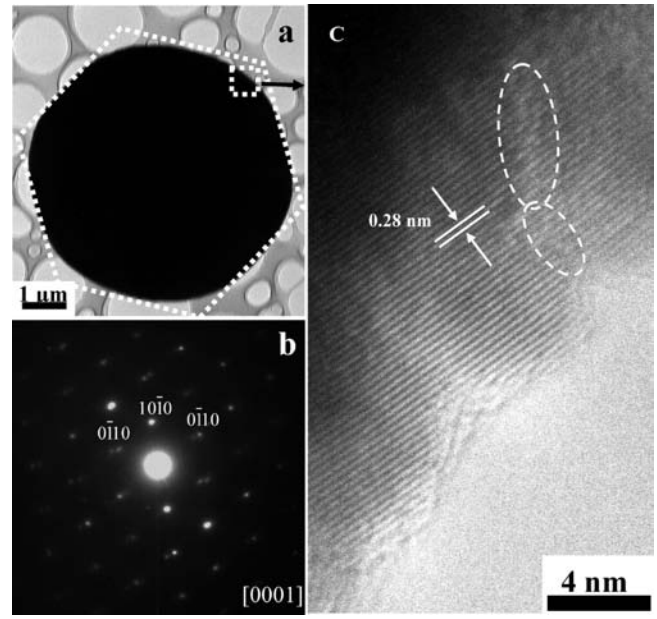

Figure 2. (a) TEM image of a single ZnO microsphere. (b) [0001] zone-axis SAED pattern obtained from the rim of the microsphere (with the incident electron beam normal to the nanoplatelet in (c). (c) HRTEM image of the edges of the microsphere marked in (a). The white circles point to the mesopores and defects.

circles).[11−16,33] The distinctive mesocrystal structure consisting of many polar faces suggests that the stacking pattern may arise from its intrinsic dipole moment and has promising applications in photocatalysis because the polar faces of ZnO have the highest photocatalysis efficiency among all faces.[25]

To further explore how such a superstructure is assembled, time-dependent experiments are performed. The p-XRD data reveal that the coherence lengths of D_{002} are nearly constant during the growth of the superstructure, suggesting that the formation of the mesocrystals is based on nonclassical crystallization (Figure SI-2).[15] The morphological evolution is examined by FE-SEM, and the results are shown in Figure 3. After reacting for 3 h, a novel apple-like nanoplatelet-based ZnO structure with two holes on its poles is observed. The nanoplatelets are also well aligned forming the apple-like structure, which is reported for the first time in ZnO (Figure 3a). The apples have an average diameter of 3 μm. In the FE-SEM image, although none of the apples directly shows two holes, the fact that every apple has a hole on it and some apples have a concave characteristic on both poles (the white arrows) indicates the existence of two holes. The nanoplatelets surround the hole according to the assembly pattern mentioned above. In addition, it can be seen that the apple has a more distinct hexagonal shape (the inset of Figure 3a) than the product after reacting for 10 h. When the reaction time is increased to 5 h, some apples grow bigger but without holes and some small ones still have typical holes (Figure 3b). This result suggests that the microsphere is evolved from the apple-like structure and also rules out the possibility of the etching mechanism.[34] Figure 3b further illustrates that the holes gradually vanish by filling with loosely packed nanoplatelets. When the reaction time reaches 7 h, some microspheres become bigger and grow into densely packed ones.

(33) Zhou, L.; Boyle, D. S.; O'Brien, P. *J. Am. Chem. Soc.* **2008**, *130*, 1309–1320.
(34) Li, F.; Ding, Y.; Gao, P. X.; Xin, X. Q.; Wang, Z. L. *Angew. Chem., Int. Ed.* **2004**, *43*, 5238–5242.

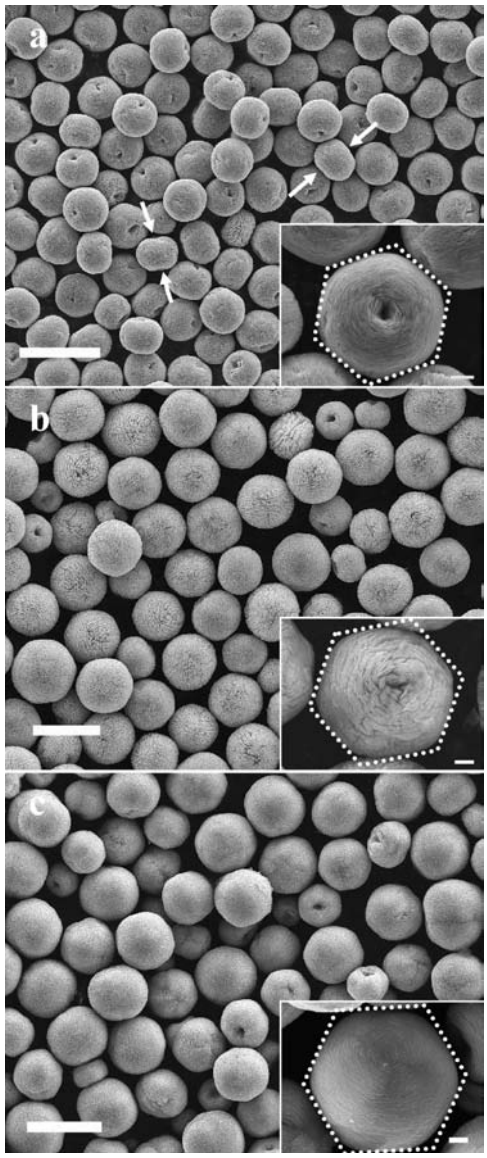

Figure 3. Growth morphology of the ZnO microsphere as a function of the reaction time: (a) 3, (b) 5, and (c) 7 h. The inset is the representative microsphere in each sample. Scale bar: 5 μm in (a) to (c) and 500 nm in the insets.

The apple-like structures gradually disappear (the inset of Figure 3c). Our observation that the unique holes on both poles vanish easily strongly suggests that this nonclassical crystallization process is due to the long-range electric field.[20]

With regard to the formation of the fluoroapatite−gelatin nanocomposites, Kniep et al. have reported morphogenesis from the hexagonal-prismatic seed to a slightly notched sphere.[4] Experimental evidence and theoretical calculation disclose that the morphogenesis of the biocomposite has a close relation with the mesoscopic dipole field generated by the parallel alignment of dipolar triple-helical protein fibers in the initial seed structure.[22,35−38] In the current case, considering the unique hole

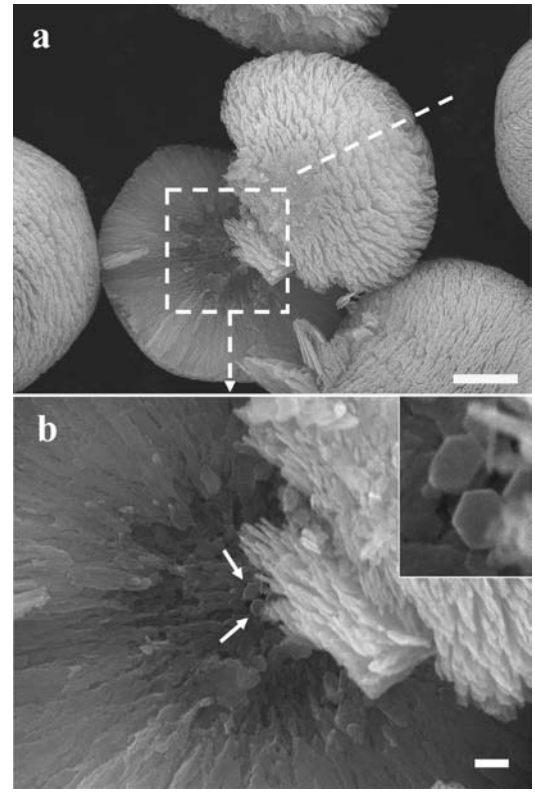

Figure 4. (a) A cracked microsphere in the 5 h product. The dashed line is the axis of the microsphere. (b) The detailed inner structure of the cracked microsphere. The arrows point to the distinct individual nanoplatelets on the surface. The inset is the magnified figure of the area that the arrows point to. Scale bar: (a) 1 μm and (b) 200 nm.

structure on the poles[20] and the fact that the dipole−dipole interaction between the nanoplatelets commonly causes anisotropic stacking along the *c*-axis,[39] we speculate that there may also be a core which controls the assembly to construct the spherical superstructure. A cracked microsphere found in the product shows the inner structure of the microspheres, and the corresponding SEM image presented in Figure 4a shows a clear boundary in the center region of the microsphere. It is separated from the outer radial structure and inner nonradial structure, indicating the existence of a core structure. The outer radial structure grows with radial alignment pointing to the inner core center, and the inner core shows nonradial streaks. The different streaks suggest different ways of assembly for the core and outer shell. High magnification SEM observation of the fractured core surface reveals small hexagonal nanoplatelets on the surface of the core (the white arrows and the inset in Figure 4b). According to the 6-fold symmetry of the nanoplatelet, it can be concluded that it has (0001) top/bottom faces. The rough surface of the core rules out the possibility of a single crystal with the expected typical cleavage plane reported before.[30] Obviously, further growth of the radial structure is strongly affected by the inner core.

Though many nanoplatelets on the core are fused together during the growth process, according to these small unfused platelets and their distinctive alignment, it can be inferred that the core is formed through the mesoscale assembly of hexagonal nanoparticle building units along the *c*-axis. In fact, we have

(35) Busch, S.; Dolhaine, H.; DuChesne, A.; Heinz, S.; Hochrein, O.; Laeri, F.; Podebrand, O.; Vietze, U.; Weiland, T.; Kniep, R. *Eur. J. Inorg. Chem.* **1999**, *10*, 1643–1653.
(36) Busch, S.; Schwarz, U.; Kniep, R. *Adv. Funct. Mater.* **2003**, *13*, 189–198.
(37) Simon, P.; Schwarz, U.; Kniep, R. *J. Mater. Chem.* **2005**, *15*, 4992–4996.
(38) Paparcone, R.; Kniep, R.; Brickmann, J. *Phys. Chem. Chem. Phys.* **2009**, *11*, 2186–2194.

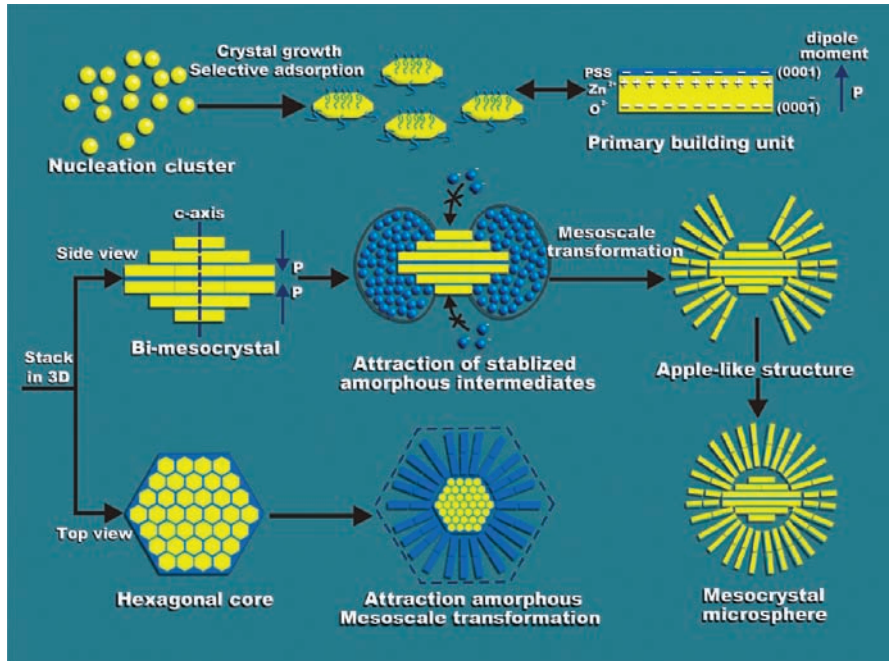

Figure 5. Schematic illustration of the growth model.

found that the axis of the microsphere is equal to the *c*-axis of the core, and the holes are formed in the *c*-axis direction. The hexagonal shape is distinctive when observing the structure from the *c*-axis direction. Cölfen et al. have reported a unique convex-concave morphology in the $CaCO_3$ mesocrystal in which the long-range dipolar interactions control the growth of the mesoscale assembly.[20] From the above results, a plausible growth mechanism can be postulated to explain the formation of the core−shell mesocrystal microsphere based on the two kinds of electric fields as described in Figure 5.

A large number of precursor particles are first formed due to supersaturation in the solution. Because the polymer poly(sodium 4-styrenesulfonate) (PSS) has negatively charged sulfonic acid groups in the side chain, the PSS will anchor on the Zn^{2+}-terminated (0001) plane to suppress the *c*-axis growth due to the strong charge interaction.[31] Adsorption of the PSS changes the intrinsic anisotropy in the growth rate and makes the nanocrystals to grow preferentially along the [10$\bar{1}$0] direction to form stable and thin colloidal hexagonal nanoplatelets. In this stage, the nanoplatelet with polyelectrolyte stabilizes the Zn^{2+} face on one side but does not do so on the O^{2-}-terminated face on the counter side. Since the negative charges on the polymer-adsorbed thin layer are not enough to change the dipolar field caused by the positive and negative charge separation from a nanoplatelet thickness of ∼10−20 nm, such a nanoplatelet structure has a strong dipole moment along the *c*-axis.

Adsorption of the polymer leads to growth by aggregation of the nanoparticles rather than coarsening. As the nanoplatelets exhibit a single directional polar field, such dipolar nanoplatelets will twin together on the (0001) planes to counterbalance the dipole field with the PSS for charge neutralization and plane stabilization.[40] Meanwhile, they act as building units to align in three dimensions to minimize the mutual interaction energy according to the self-similarity rule for forming a hexagonal bimesocrystal with (0001) planes as the juncture. This process is driven by the screened anisotropic potential, and the polymer may act as a matrix for the oriented crystallization of inorganic building units.[13,33,36,37] The twinning phenomenon with the (0001) or (000$\bar{1}$) plane as the juncture occurs commonly in ZnO.[31,34,40,41] In the aggregation, stacking along the *c*-axis can happen only nanoplatelet by nanoplatelet because other twinned structures with the (000$\bar{1}$) plane will be repelled by the stacked nanoplatelet with the (000$\bar{1}$) plane due to electrostatic repulsion. When adding all the microscopic dipoles, a unique twinned macroscopic electric dipole system is formed acting as a core to determine the growth of the spherical superstructure.

The macroscopic electric dipole system attracts not only the dipolar nanoplatelets but also the polymer-stabilized intermediates in three dimensions after the bimesocrystal has reached a critical size.[20] Since the PSS is negatively charged, the polymer-stabilized amorphous intermediates in the solution carry the homogeneous negative surface charges to aggregate around the hexagonal bimesocrystal under the action of its electric field. Because of electrostatic repulsion, the negatively charged amorphous intermediates cannot land on the middle of the similarly charged (000$\bar{1}$) planes on both poles, thereby giving rise to the holes formed on both sides along the *c*-axis.

The stable aggregated amorphous intermediates crystallize and assemble into an orderly shell structure via mesoscale transformation. They also exhibit the preferred thin nanoplatelet shape for selective adsorption of the PSS (Figure 1d). These nanoplatelets formed on the outer part also possess a dipole field. Under the synergistic effects of the electric field generated by the core (3D directions) and the dipole−dipole interaction (linearly along the *c*-axis of the nanoplatelet), the nanoplatelets on the outer part become parallel to each other and reorient where the electric field is normal to their polar faces on account of electrostatic interaction during the transformation. This is

(39) Tang, Z. Y.; Kotov, N. A.; Giesig, M. *Science* **2002**, *297*, 237–240.
(40) Jia, L. C.; Cai, W. P.; Wang, H. Q.; Zeng, H. B. *Cryst. Growth Des.* **2008**, *8*, 4367–4371.
(41) Zhang, J. H.; Liu, H. Y.; Wang, Z. L.; Ming, N. M.; Li, Z. R.; Biris, A. S. *Adv. Funct. Mater.* **2007**, *17*, 3897–3905.

believed to be the main driving force for the stacking phenomenon around the *c*-axis forming the radial surface with good alignment. The hexagonal shape in the early stage (view from *c*-axis) confirms the aggregation mechanism based on the hexagonal core (the inset of Figure 3a).

As the reaction time increases, the particle grows and the electric field generated by the core is gradually counterbalanced by the electric field from the nanoplatelet on the shell. The holes vanish via further attachment of the nanoplatelets near the hole. At this stage, the electric field of the core is basically screened by the shell. The core-based electric field controlled growth is replaced by energetically favored aggregation and dipole−dipole interaction to lower the total energy of the structure. As a result, the microsphere structure transforms from a hexagonal to a more spherical shape to minimize the total energy and the loosely packed surfaces morph into densely packed ones to reduce the exposed high energy planes as the reaction time is increased.[42,43] Finally a nanoplatelet-based, core−shell mesocrystal microsphere is formed. This growth mechanism can also be used to explain the formation of the doughnut ZnO structure with a hole only on one side reported recently.[38,39] However, in the previously reported structure, the untwinned single hexagonal plate acts as the core to control further stacking of the nanoplatelets which can induce only one concave−convex structure.

It seems that the structures of the samples before 3 h are important in determining the apple-like superstructure from the seed structure. Figure 6a to 6d show the initial stage morphologies of the samples before 3 h, and Figure 6e depicts the corresponding XRD patterns. In the sample after 30 min growth, some large particles occur without obvious superstructures. The p-XRD result shows that these particles have compositions of $Zn(OH)_2$. This is because the HMT releases OH^- ions at elevated temperature in the initial stage.[44,45] As the growth time increases, some sphere-like structures with a hole on each sphere appear (Figure 6b). Their sizes are larger than those of the apple-like superstructure formed subsequently. The surfaces of these spheres are rough, and the particles on them arrange randomly (inset). The p-XRD pattern shows the formation of a partial crystalline ZnO structure because of the dehydration of $Zn(OH)_2$.[46] The existence of the holes suggests that a core has been formed within a sphere and the core-based electric field starts to take effect. This is consistent with the process shown in Figure 5. When the growth time increases to 110 min, the biconcave structure which is the premorphology of the apple-like structure appears and its composition completely becomes pure ZnO (Figure 6c and 6e). During the mesoscale transformation, the shell structure has a large change. The evolution from the loosely packed aggregation of the polymer-stabilized intermediates [amorphous ZnO and $Zn(OH)_2$] into the densely packed well crystallized ZnO nanoplatelets leads to a large reduction in the superstructure size. The stacking pattern of the biconcave structure is the same as that described above, and the presence of a crevice on each biconcave structure confirms

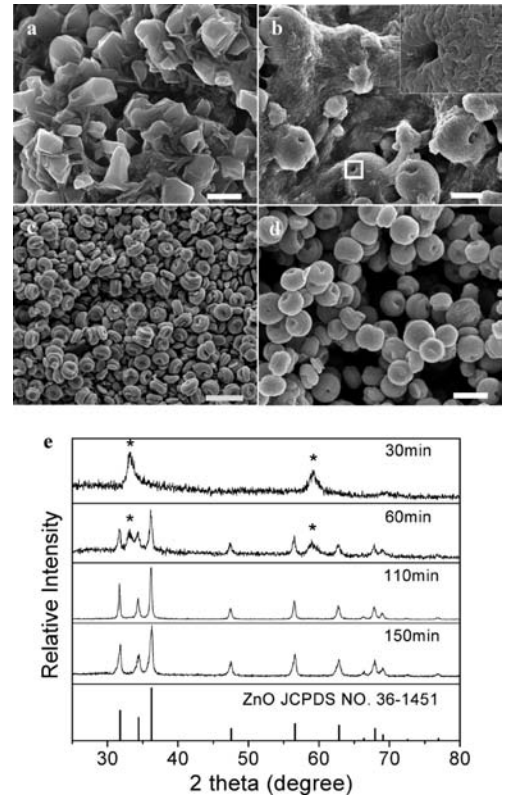

Figure 6. Initial stage morphologies of the samples before 3 h. The growth times of the samples are (a) 30, (b) 60, (c) 110, and (d) 150 min. The inset in (b) shows a locally magnified image of the sphere surface (marked with a solid white rectangle). (e) Corresponding p-XRD patterns. The label (*) points to the diffraction peaks from $Zn(OH)_2$ (JCPDS card no. 72-2032). Scale bars: 5 μm in (a) and (b) and 2 μm in (c) and (d).

the juncture of the cores. Further attachment of the nanoplatelets under the electric field effect leads to the formation of the not fully grown apple-like structure (Figure 6d). The coherence lengths D_{002} of the samples precipitated in 110 and 150 min are 15.1 and 15 nm, respectively, suggesting that the building units of the samples before 3 h also have the same homogeneity.

Previous investigation has indicated that some charged dyes can help to assess the electric polarity of the structure.[20,31] Here, to verify the twinned-dipolar characteristics of the apple-like structure, which plays a crucial role in the intrinsic dipole-field-driven mechanism, a staining experiment was conducted (Figure SI-3). When the pure sample is observed under an optical microscope, there is no color on the holes and surface of the mesocrystals (Figure 7a and 7b). When the samples are mixed with negatively charged dye (Congo Red, Figure SI-3a), few surfaces of the mecocrystals are stained red (Figures 7c and 7d). This suggests that the negatively charged dye molecules are hardly attached onto the mesocrystals, especially the holes. When the positively charged dye (Safranine T, Figure SI-3b) is used, however, the mesocrystals are stained red, especially near the hole (Figure 7e and 7f). As indicated in Figure 5, the surface sections around the holes are negatively charged because the up and down sides of the core are O^{2-}-terminated faces and the outward planes of nanoplatelets facing the holes are Zn^{2+}-terminated faces covered with the negatively charged polymer. Hence, at the surfaces near the holes, only the positively charged dye can absorb on the mesocrystal (Figure 7f). Here, we would like to point out that the two kinds of charged dyes can both land slightly onto the neutral planes such as $\{1\bar{1}00\}$ side surfaces on the shell. Therefore, some mecocrystals stained with negative

(42) Liang, J. B.; Liu, J. W.; Xie, Q.; Bai, S.; Yu, W. C.; Qian, Y. T. *J. Phys. Chem. B* **2005**, *109*, 9463–9467.
(43) Ghoshal, T.; Kar, S.; Chaudhuri, S. *Cryst. Growth Des.* **2007**, *7*, 136–141.
(44) Govender, K.; Boyle, D. S.; Kenway, P. B.; O'Brien, P. *J. Mater. Chem.* **2004**, *14*, 2575–2591.
(45) Gao, X. D.; Li, X. M.; Yu, W. D. *J. Phys. Chem. B* **2005**, *109*, 1155–1161.
(46) Yan, X. D.; Li, Z. W.; Chen, R. Q.; Gao, W. *Cryst. Growth Des.* **2008**, *8*, 2406–2410.

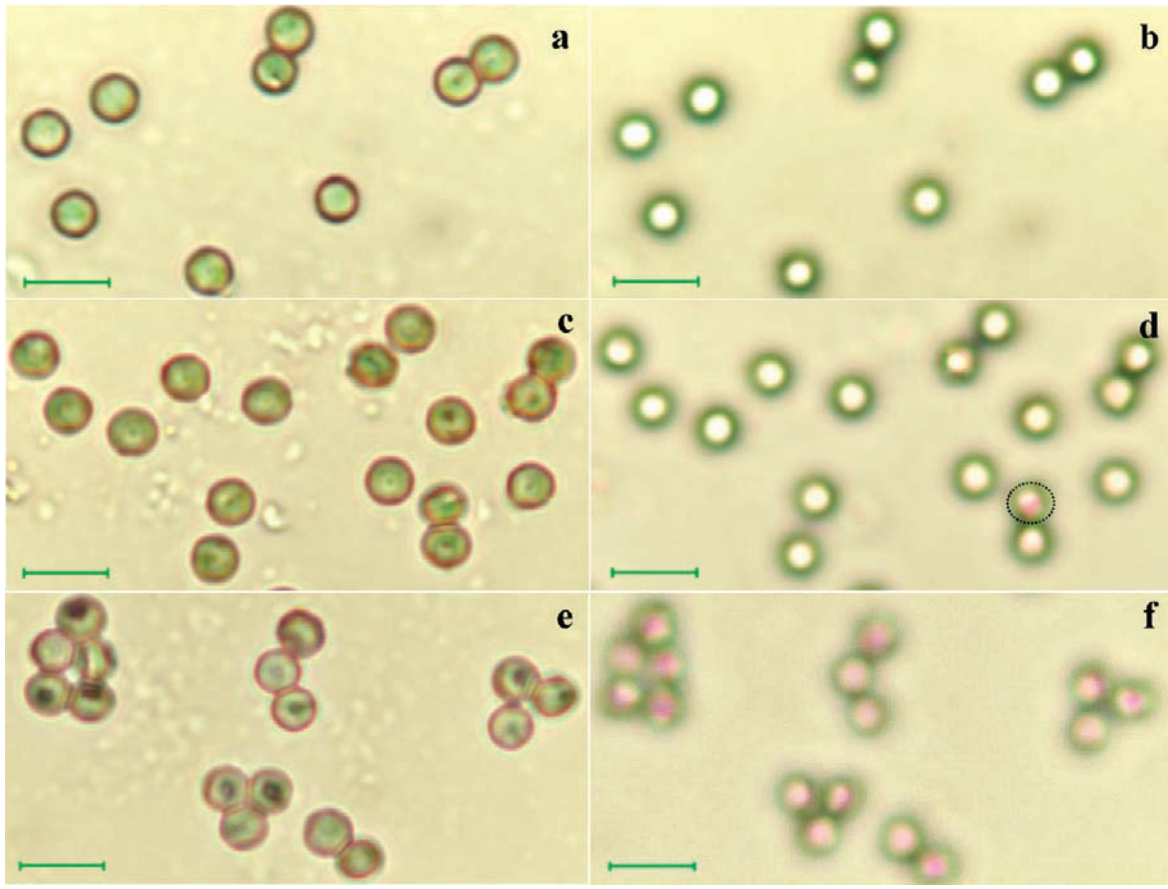

Figure 7. Optical microscopy images of the ZnO mesocrystals on the glass slips. (a and b) Pure apple-like ZnO sample without staining. (c and d) The apple-like ZnO sample stained with the negatively charged dye (Congo Red). (e and f) The apple-like ZnO sample stained with the positively charged dye (Safranine T). In these images, (a), (c), and (f) are obtained by putting the holes on the mesocrystals into the focus, which show clear morphologies of the holes on the mesocrystals. The red ring outside every mesocrystal is the diffraction fringes of the microsphere, not the dye we used. Images (b), (d), and (f) are taken by focusing the surfaces of the microspheres where the dye molecules can be judged whether they have been attached on the mesocrystals. The staining experiment is conducted on the 3 h sample. Scale bar: 5 μm.

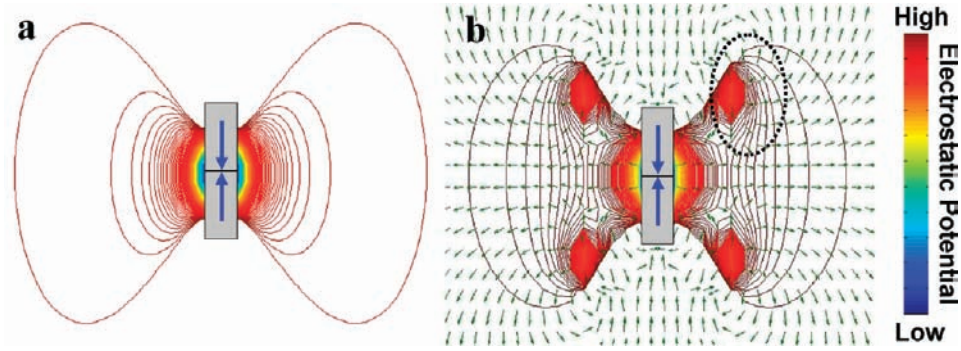

Figure 8. (a) Contour plot of the electrostatic potential distribution (color lines) around the model prism. The model prism (the gray rectangle) consists of permanent dipoles (the blue arrows). (b) The electric field (green arrows which also represent the dipoles) and electrostatic potential distributions of the model prism, which takes the dipoles of the nanoplatelets on the shell into consideration (see Figure SI-5). The green arrows indicate how the nanoplatelets are surrounding the core, because the spatial orientation of a nanoplatelet is normal to its dipole. The electric field distribution near the dipoles, which stand for the intrinsic dipoles of nanoplatelets near the hole, is marked by the black dashed circle. The color chart represents the intensity of the electrostatic potential. The distribution is shown in the $Y-Z$ plane. All the data to calculate the electric potential are used as natural units.

charges also exhibit a slight red color, as shown in Figure 7d (the dashed black circle). These results directly illustrate the charged feature of both the nanoplatelets and the apple-like structure further confirming the intrinsic dipole-driven mechanism for the superstructure formation.

A dipole-based theoretical calculation is also performed to corroborate the intrinsic dipole-driven assembly mechanism. The model is consistent with the growth mechanism that all the dipoles align along the *c*-axis and twin together with the positively charged (0001) planes as the juncture. Since we cannot obtain detailed data of the core, we simplify the core structure by using the elementary dipoles (Figure SI-4a). Figure 8a shows a contour plot of the distribution of the electrostatic potential by means of isopotential lines on the $Y-Z$ plane as calculated by the core dipole model. Since the polymer-stabilized negatively charged amorphous intermediate aggregation obeys

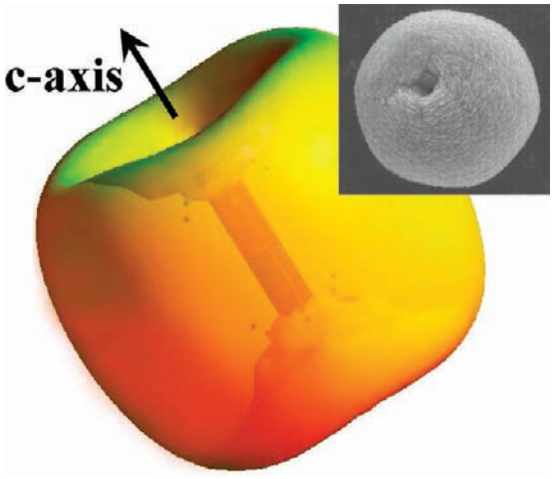

Figure 9. Calculated morphology of the three-dimensional electrostatic potential distribution. For comparison, the inset shows the observed apple-like ZnO structure obtained from the 3 h product. The black dots in the apple represent the dipoles in the model (Figure SI-5).

the minimum energy principle, the particles first favor landing on the region where the potential is low (the blue region) and then on the high potential region (the red region). As the potential increases, two holes gradually form at both sides of the prism at the *c*-axis direction, which is consistent with the experimental data. This process is also validated by the Monte Carlo method (Figure SI-4b). When the amorphous intermediates start to crystallize into ZnO nanoplatelets, the dipole−dipole interaction between the nanoplatelets should be taken into consideration (Figure SI-5). Figure 8b shows how the dipoles in the shell arrange to surround the core. Obviously, the symmetric dipoles in the shell introduced affect the directions of other dipoles nearby (dashed black circle). It is very different from the situation which only considers the role of the core (Figure SI-6). Under the synergistic effect of the two electric fields, the nanoplatelets in the shell will obey the plotted assembly pattern when they are stacking to fill the holes or reorienting in the shell. This is consistent with the experimental data shown in Figure 1c and 1d. The 3D image in Figure 9 shows the theoretical calculation morphology stipulated by our model. The calculated apple-like morphology is the same as that of the superstructure observed after reacting for 3 h (the inset in Figure 9).

4. Outlook

Nanoplatelet-based, core−shell ZnO mesocrystal microspheres with a uniform size have been synthesized via a one-step hydrothermal process at low temperature. The ZnO microsphere assembly is formed from 2D nanoplatelets driven by the intrinsic dipole field. It stems from the synergistic effect of two kinds of electric fields leading to the formation of the spherical core−shell superstructure. The strategy that uses a polyelectrolyte to design the anisotropic charged building units is a promising technique to fabricate more complex functional materials and mesocrystals.

Acknowledgment. This work was supported by the National and Jiangsu Natural Science Foundations (Nos. BK2006715, BK2008020, and 60676056). Partial support was also from National Basic Research Programs of China under Grant Nos. 2007CB936300 and 2006CB921803 as well as Hong Kong Research Grants Council (RGC) General Research Grant (GRF) No. CityU 112307.

Supporting Information Available: Figure SI-1: Powder X-ray diffraction pattern of the ZnO nanoplatelet-based mesocrystal microspheres obtained from the 10 h product. Figure SI-2: P-XRD patterns of the samples prepared at different reaction periods. Figure SI-3: The chemical structures of anionic Congo Red and cationic Safranine T. Figure SI-4: Core dipole model consisting of charge (positive or negative) distribution at twenty-one positions on the prism and Monte Carlo simulation of the process that the polymer-stabilized negatively charged amorphous intermediates aggregate under the electric field of the core. Figure SI-5: Model containing eight symmetric permanent dipoles surrounding the core model prism. Figure SI-6: Electric field and electric potential distributions of the core model prism. This material is available free of charge via the Internet at http://pubs.acs.org.

JA9039136